

Pathways for efficiency improvements of industrial PERC silicon solar cells

Nagarajan Balaji ^{*}, Donny Lai, Vinodh Shanmugam, Prabir Kanti Basu, Ankit Khanna, Shubham Duttagupta, Armin G. Aberle

Solar Energy Research Institute of Singapore, National University of Singapore, Singapore 117574, Singapore



ARTICLE INFO

Keywords:
PERC
Passivated contacts
Loss analysis
Laser ablation
Selective emitter

ABSTRACT

The global manufacturing capacity of Passivated Emitter and Rear Cell (PERC) devices on *p*-type Czochralski-grown silicon (Cz-Si) wafers is increasing rapidly. This paper analyses various industrial process improvements carried out in our lab to improve the efficiency of large-area Cz-Si PERC solar cells from 20.7% to 21.9%. The key improvements presented in this paper include the transition from line to dot-shaped laser openings in the rear dielectric stack, a dual printing approach for the front fingers and implementation of a laser-doped selective-emitter structure. A nanosecond (ns) pulsed laser source with 532 nm wavelength was used for both the rear dielectric ablation and the front laser doping. By adopting a systematic power loss analysis approach and targeting the largest power loss mechanisms at various stages of development, the best efficiency of the solar cells in this experimental study was improved from 20.7% to 21.9%. Pathways for further improvements in efficiency are analysed, including the application of passivated-contact structures in a PERC-like cell.

1. Introduction

The Passivated Emitter and Rear Cell (PERC) device on *p*-type Cz-Si wafers and with screen-printed front and rear contacts is presently the dominant industrial solar cell type (ITRPV, 2019). The global production capacity of PERC cells was less than 1 GW in 2014 and has since grown to more than 60 GW in 2019 (F. Colville, 2019). This dramatic growth in PERC production capacity over the last 5 years was accompanied by continuous cell and module efficiency improvements. Typical PERC efficiencies in 2012 on Cz-Si were around 19% (Basu et al., 2012; Glunz et al.), while the median efficiency of PERC in production is now typically in the range of 21.7–22.2% (Dullweber et al., 2016; Dullweber and Schmidt, 2016; Lv et al., 2020; Müller et al., 2017; Werner et al., 2017; Wu et al., 2018). This efficiency gain was possible due to improvements of materials and technologies associated with various process steps of PERC fabrication, e.g., the wafer bulk quality (Yichun and Tian, 2018), inline wet-chemical single-side polishing (Kranz et al., 2013; Strintz et al., 2017), phosphorus emitter with lower saturation current density (J_{0e}) values (Shetty et al., 2013; Wagner et al., 2016), metal pastes and screens (Lorenz et al., 2018; Shanmugam et al., 2014), rear surface passivation, rear laser ablation (Ali et al., 2019; Preu et al., 2000), and the selective-emitter process (Werner et al., 2017; Wu et al., 2018). In 2019, LONGi Solar announced a world-record PERC efficiency of 24.06% (Mark Osborne, 2019; Mark Hutchins, 2018; Mark Osborne,

2020; Emiliano Bellini, 2020). However, this R&D record PERC cell included processes (such as inverted pyramids as front surface texture) and materials (such as *p*-type Si wafers with a bulk lifetime in excess of 1.5 ms) that are currently too expensive for use in mass production (F. Jianbin, 2019).

Screen printing technology is the dominant metallization process for industrial silicon wafer solar cells and is also a well-established process for contacting phosphorus diffused emitters. Previously, screen-printed Ag pastes required heavily doped phosphorus emitters to achieve a good ohmic contact, and this in turn directly limited the efficiency of the solar cells. A highly doped phosphorus emitter on the front results in a poor response to short wavelengths (blue response) due to increased recombination in the emitter (Cuevas and Russell, 2000). Screen printed Ag pastes have improved drastically in contacting phosphorus diffused emitters with lower surface doping concentrations. As the emitter becomes less doped and thinner, emitter saturation current density of the contacted area increases and hence the metallisation induced recombination losses increases (Shanmugam et al., 2016). The selective emitter (SE) approach addresses all these issues: (1) having a heavily diffused emitter just under the screen-printed metal contact helps in reducing the contact resistance and the metallisation induced recombination losses, (2) a lightly doped phosphorus emitter in the non-metallised regions ensures a good blue response and lower emitter recombination. These improvements result in a 0.3–0.4% absolute gain in PV efficiency over

* Corresponding author.

E-mail address: serbn@nus.edu.sg (N. Balaji).

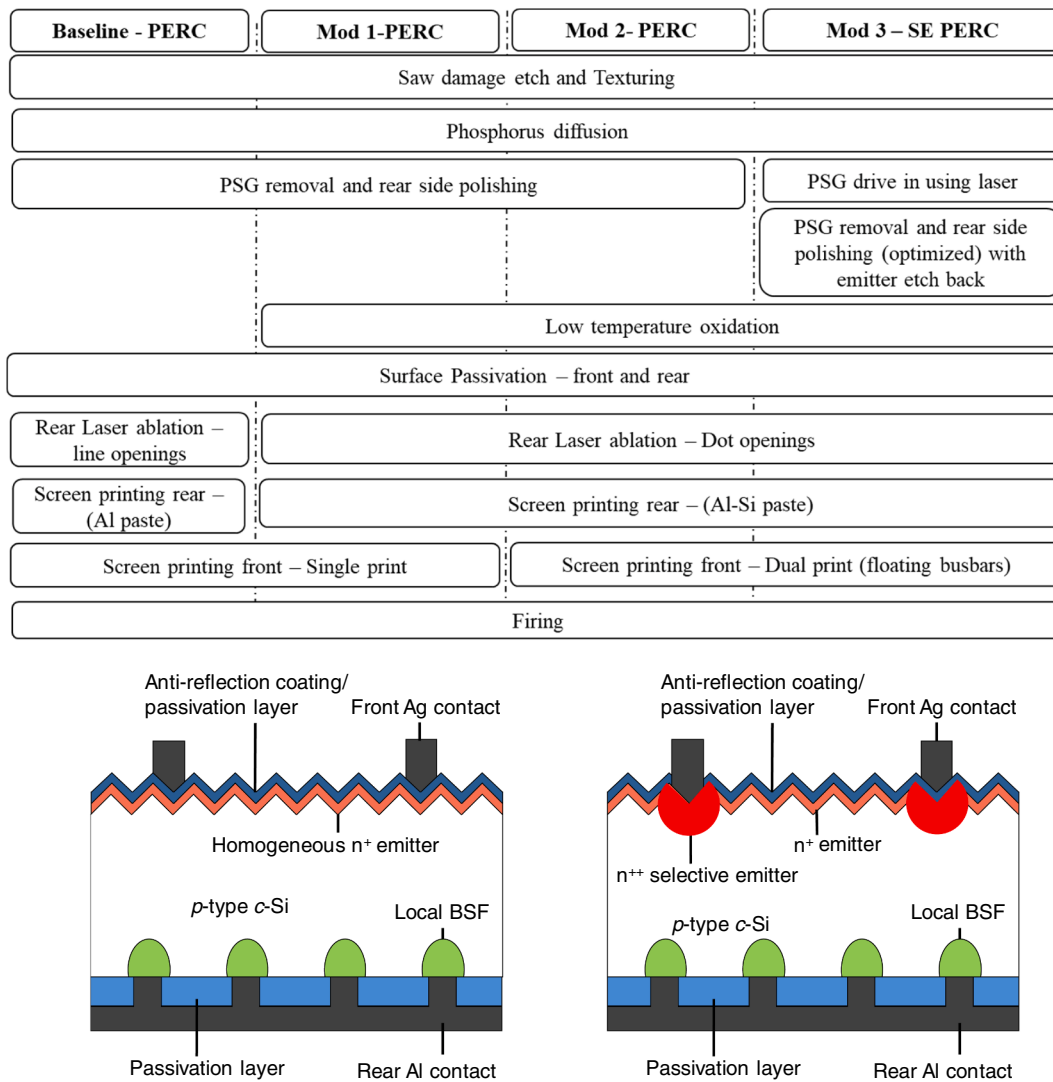


Fig. 1. Process flow for the fabrication of PERC solar cells and the various process modifications, along with the schematic of the baseline PERC and SE PERC solar cell fabricated in this study.

standard PERC cells with homogeneous phosphorus emitter. The interest in selective emitter (SE) PERC cells has been rising in the last few years and is now being commercially mass produced. There are many different approaches for SE formation such as laser doping using PSG (Röder et al., 2009), laser chemical processing (LCP) (Kray et al., 2008), dopant inks (Antoniadis et al., 2010), laser doped selective emitter approach (LDSE) (Hallam et al., 2015), patterned diffusion or implantation using a patterned dielectric layer (Dubé et al., 2011), inkjet masking and etch-back method (Dastgheib-Shirazi et al., 2008; Lauer-mann et al., 2009).

The fabrication of selective emitters by laser processing has gained significant interest due to its inherent advantages such as high throughput processing, versatility, and precision. The influence of the laser beam profile (Gaussian, top-hat, or line laser beam) on the doping process has been investigated by several groups (Jäger et al., 2010; Röder et al., 2010; Safiei et al., 2013). In case of the focused Gaussian laser beam profile, the Gaussian intensity distribution results in inhomogeneity of doping within a laser spot and damages the textured pyramids (Safiei et al., 2013). A top-hat laser beam profile results in homogeneous laser doping and is widely used in the PV industry for laser doping applications.

This paper presents a very systematic efficiency improvement study experimentally achieved in our lab with several industrially feasible

PERC improvements, leading from a baseline PERC efficiency of 20.7% to improved PERC devices with 21.9% efficiency. A systematic loss analysis is carried out to identify the largest power loss mechanisms in the 21.9% cells and identify pathways for further efficiency gains, including the application of passivated-contact structures in a PERC-like cell.

2. Experimental details

In this study, commercial large-area (244 cm^2) p-type pseudo-square Cz-Si wafers with $0.5\text{--}1 \Omega\text{cm}$ bulk resistivity were used. The process flow for the fabrication of baseline PERC solar cells is shown in Fig. 1. The wafers were saw damage etched, and then textured on both sides using an IPA-free solution to generate a random-pyramid surface texture, followed by a standard wet-chemical cleaning sequence: Radio Corporation of America (RCA) clean 1 and 2, followed by a dip in dilute HF. The wafers then went through a phosphorus diffusion process using phosphorus oxychloride (POCl_3) in a commercial horizontal tube diffusion furnace (Quantum, Tempress) resulting in a sheet resistance of about $90 \Omega/\text{square}$. Rear-side etching and phosphosilicate glass (PSG) removal were carried out using an inline single-side etching tool (Linea Pilot, Singulus). This baseline etching process does not fully remove the rear surface texture. The wafers were then passivated on both sides (in 2

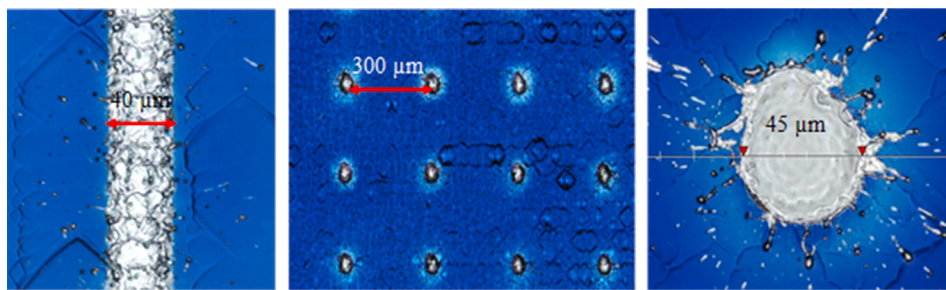


Fig. 2. 2D optical image of the laser ablation pattern. 40 μm line ablation at a spacing of 850 μm (baseline), 45 μm dot ablation at a pitch of 300 μm (Mod-1).

separate runs) using a plasma-enhanced chemical vapour deposition (PECVD) process in a commercial inline PECVD tool (MAiA, Meyer Burger). The rear side was passivated with a PECVD stack of aluminium oxide (AlO_y) and silicon nitride (SiN_x) with a thickness of 20 nm and 100 nm, respectively. The front side was passivated with a 70 nm PECVD SiN_x layer. The rear $\text{AlO}_y/\text{SiN}_x$ stack was then locally ablated using a nanosecond (ns) green laser (ILS500T, Innolas). The wafers were then screen printed with Al paste (DuPont, PV36S) on the rear. The front grid consisting of 105 fingers and 5 busbars (each 700 μm wide) was screen printed using a commercially available Ag paste (DuPont, PV 21). The samples were then fired using an industrial fast firing furnace (BTU, Sinterra) at a peak temperature of 730 °C. Fig. 1 also shows the process flow for the PERC cells from different groups fabricated in this study. The modifications to the baseline process flow are discussed in Section 3.

2.1. Characterization methods

The phosphorus diffused emitters were characterized using a 4-point probe (SR2000 N, AIT Instruments) to determine the sheet resistance and an electrochemical capacitance-voltage (ECV) profiler (CVP21 Profiler, WEP Control) to determine the dopant profile. It is noted that ECV merely measures the electrically active dopants, and thus the actual dopant concentration is higher than the ECV result. The cells' implied V_{oc} was measured using the quasi-steady-state photoconductance (QSSPC) method (WCT-120, Sinton Instruments) on unmetallised cell precursors (Kerr et al., 2002). J_{oe} of the phosphorus emitters was determined using the high injection method proposed by Kane and Swanson (Kane and Swanson, 1985). The photoluminescence (PL) images for the loss analysis were taken with a commercial PL imaging system (BT Imaging) using a 915-nm laser as the excitation source. The current-voltage measurements of the solar cells were done using a Class AAA-rated LED-based flash tester (Sinus-220, Wavelabs) calibrated using a reference cell calibrated by Fraunhofer ISE's CalLab. For the current loss analysis in the fabricated solar cells, the spectral response (SR) and the reflectance of the cells was measured with a single-point spectral response system (PVE300-IVT, Bentham).

3. Results and discussion

The baseline PERC process shown in Fig. 1 resulted in a peak efficiency of 20.8% in our lab. After establishing this baseline process, three improvements were carried out to improve the cell efficiencies. These improvements will be referred to as modifications (Mod) 1–3.

3.1. Process modifications

Modification 1 (Mod-1) focused on optimizing the rear laser ablation pattern and the rear metallisation process. In addition to these two changes, a low-temperature oxidation step was included in the process flow, as shown in Fig. 1. After diffusion and rear-side polishing, a low-temperature oxidation process at 600 °C for 60 min was carried out on these wafers using the tube furnace. The rear dielectric ablation was

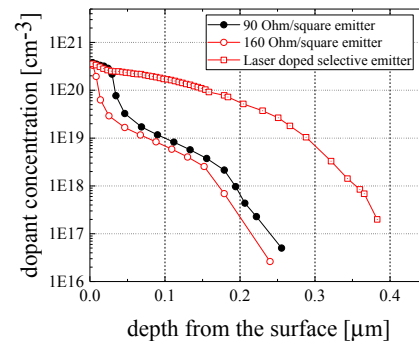


Fig. 3. Active dopant profile of the phosphorus diffused emitters. Baseline 90 Ω/square (as diffused emitter), 160 Ω/square (emitter after laser damage etch), and the 45 Ω/square (after PSG laser doping under the metal contacts).

changed from a line opening pattern to a dot opening pattern, as shown in Fig. 2. This reduces the rear surface metal fraction from 5.0% (lines) to less than 2.5% (dots). It is worth mentioning here that, the common industry practice is to use laser dot contact to achieve low $J_{0,\text{met}}$ values (Tsuiji et al., 2019). The rear metal paste was changed from an Al paste to an Al-Si paste (Toyo, TL08D), as this was demonstrated in our earlier work to lead to a cell efficiency gain (Shanmugam et al., 2018). By incorporating these three changes to the baseline process, we achieved an average cell efficiency gain of 0.6% absolute, whereby the champion cell had an efficiency of 21.4% and an open-circuit voltage (V_{oc}) of 660 mV.

Mod-2 focused on the dual printing approach for the front metallisation. Dual printing is a process wherein the front busbars (BB) are printed first (using a separate screen and using a paste that is less aggressive on the SiN_x passivation layer), followed by the second print (where only the fingers are printed using the conventional fire-through Ag paste) (Ksnig et al., 2012; Shanmugam et al., 2015). This approach leads to a significant reduction in the metal recombination associated with the busbars ("floating busbars") and hence increases the V_{oc} of the solar cells. At the same time, dual printing reduces the total Ag consumption per cell because the thickness of the busbars can be reduced (by customising the busbar screens), as it is not required for the busbars to have the same thickness as the fingers (Hannebauer et al., 2013). Both the finger paste (PV21) and the floating busbar paste (PVD2B) were obtained from DuPont. The successful integration of the dual printing approach for the front grid metallisation resulted in a champion cell efficiency of 21.5%, with a V_{oc} of 663 mV.

Mod-3 focused on integrating the selective-emitter approach using laser doping of phosphosilicate glass (PSG). The nanosecond laser source used in this work emits 38 ns laser pulses at a wavelength of 532 nm and has a repetition rate in the range of 20–200 kHz. The laser source emits pulses with a Gaussian profile. The focused Gaussian laser beam profile damages the textured pyramids and results in inhomogeneous laser doping. To overcome these limitations, we defocused the Gaussian laser beam profile (Safiei et al., 2013). The laser fluence was adjusted to laser

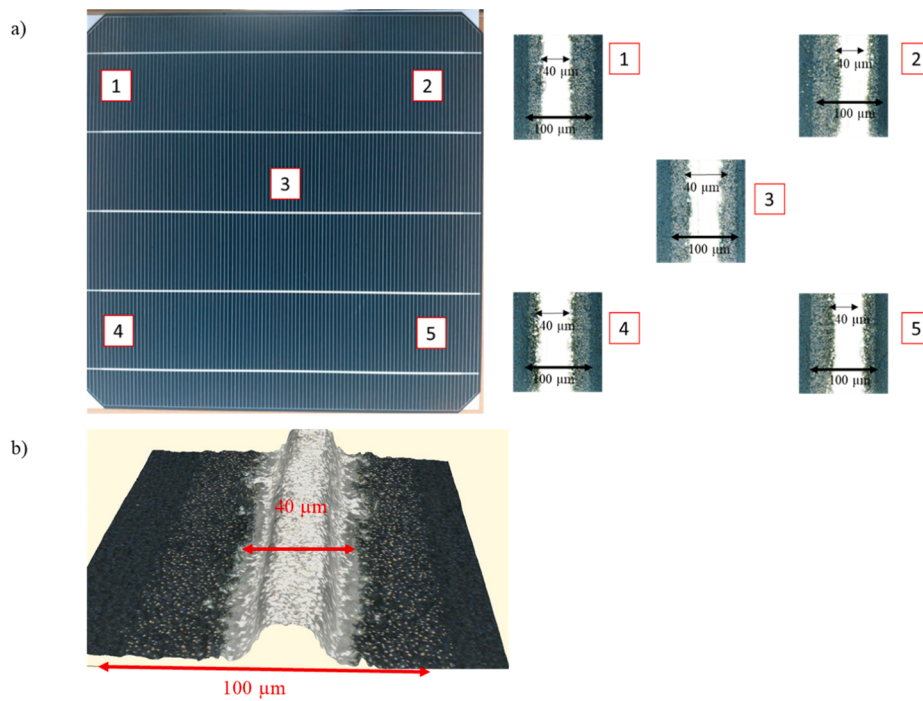


Fig. 4. Alignment between the laser doped regions and the screen-printed Ag metal paste. With the developed routine, it is possible to obtain perfect alignment between 100 μm laser doped regions and 40 μm screen printed Ag metal paste over the entire wafer. Figure a shows the alignment at 5 different points on a finished solar cell. Figure b shows the 3D profile of a printed line on the laser doped region. The slight texture deformation due to the laser doping process using a Gaussian laser spot is also visible clearly from this figure.

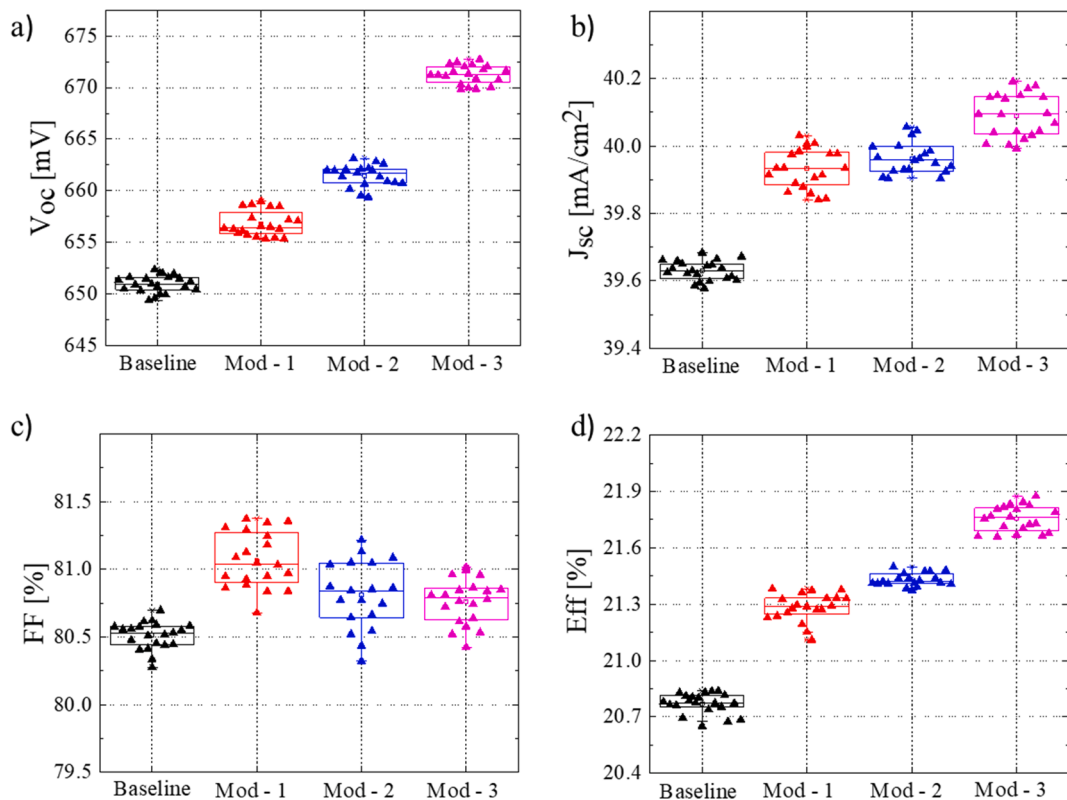


Fig. 5. I-V characteristics of the fabricated solar cells with respect to the different process modifications. Mod-1 focused on rear laser ablation and metallisation, Mod-2 focused on the optimised inline edge isolation process, and Mod-3 is the integration of the selective emitter process. The efficiency of the PERC solar cells increased from 20.8% to 21.9% with the 5-BB metallization.

dope while minimising the damage to the textured pyramids since a higher laser fluence flattens the textured pyramids and it is known that flat surfaces are difficult to contact with screen printed Ag paste. After the laser doping process, an emitter etch back process was applied using a saturated solution of NaOCl at 80 °C for 90 s. This process results in

etching the phosphorus emitter regions in the non-laser doped areas. The sheet resistance of the laser doped regions was around 45 Ω/sq , while in the non-laser doped regions after the etch back process it was around 160 Ω/sq (i.e., the baseline 90 Ω/sq emitter was etched back to 160 Ω/sq). These emitter regions were characterised by ECV profiling

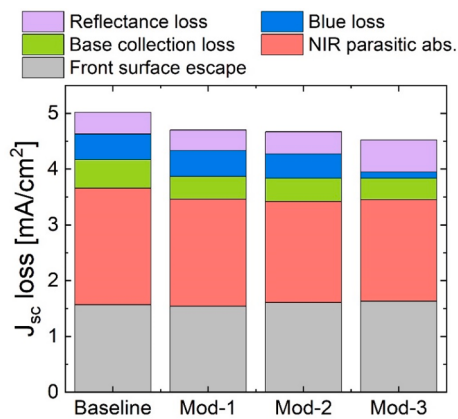


Fig. 6. Results of J_{sc} loss analysis for the cell groups. The blue loss is significantly lower for the SE-PERC (Mod-3) cells when compared to the other groups. This is due to the very lightly doped ($160 \Omega/\text{sq}$) emitter used in Mod-3, whereas all other groups use a more heavily doped ($90 \Omega/\text{sq}$) emitter. (For interpretation of the references to colour in this figure legend, the reader is referred to the web version of this article.)

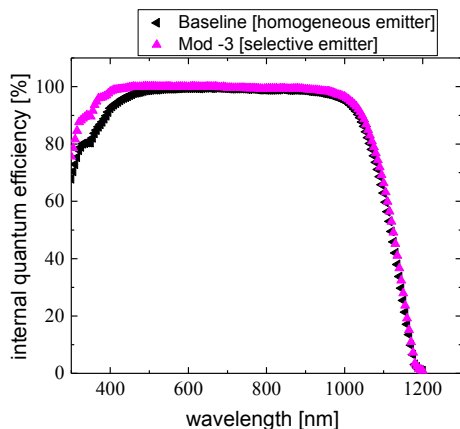


Fig. 7. IQE of the median solar cells fabricated from the baseline group with homogeneous emitter and the Mod-3 group with selective emitter. The better blue response (short-wavelength response) of the Mod-3 selective emitter group when compared to the baseline group is the reason for Mod-3 cells to have better J_{sc} values. (For interpretation of the references to colour in this figure legend, the reader is referred to the web version of this article.)

for active dopant profile measurements and is depicted in Fig. 3. After this, the wafers underwent the same process as shown in Fig. 1.

Another key aspect for the successful integration of the SE process is to ensure good alignment between the laser doped regions and the screen-printed Ag metal paste. A slight misalignment will result in significant drops in the V_{oc} and the fill factor (FF) of the solar cells. With improvement in the alignment and automation capabilities of the processing equipment (laser and screen-printing equipment) it is possible to successfully align the screen-printed Ag metal paste to the laser doped regions. We have developed an alignment routine wherein we consider the front grid pattern shift due to screen-stretch during the printing process and adjust the laser script accordingly. This is done on test samples prior to laser doping process to determine the optimized laser script for that screen design and Ag metal paste. This procedure was tested on multiple solar cell batches and accurate alignment was obtained in each case.

3.2. Solar cell results

Fig. 5 shows the 1-Sun I-V characteristics of the finished solar cells.

Fig. 5(a) shows the V_{oc} of the solar cells fabricated with respect to the different process modifications. A steady increase in the V_{oc} of the solar cells from 650 mV to 672 mV (baseline to Mod-3) clearly indicates the benefits of the various process modifications and the successful integration of the SE process. The reported V_{oc} values are in consistent with the values obtained by Wu et al., using SE process (Wu et al., 2018). Fig. 5(b) shows the short-circuit current density (J_{sc}) of the fabricated solar cells. The J_{sc} loss analysis of representative cells from each group is shown in Fig. 6 and the variation of the internal quantum efficiency (IQE) of baseline and Mod-3 is shown in Fig. 7. Improvements in the short-wavelength response of the Mod-3 (SE PERC cells) contribute to the enhancement in the J_{sc} values when compared to solar cells from the other groups. FF values around 81.0% were obtained for the process modification groups and this indicates the contacting capability of the Ag paste (DuPont, PV 21) used in this work. The contact resistivity of the Ag paste to the emitter was measured using the transfer length method (TLM), by cutting 1 cm strips (parallel to the busbars) from the finished solar cells. All groups yielded values less than $4 \text{ m}\Omega \text{ cm}^2$. For solar cells from the SE group (Mod-3), the good contact resistivity values obtained are also an indication that the laser doping process has not damaged or flattened the textured pyramids. The efficiency of the fabricated PERC cells with respect to different process modifications is shown in Fig. 5(d). The highest efficiency of 21.9% was obtained from the SE group (Mod-3) with 5-BB metallization. The efficiency gains reported here by us with different process modifications are somewhat less than the other reported values (Stenzel et al., 2019), our motivation was to demonstrate PERC cell efficiency improvement pathways available within our limited facilities, while comprehensively analysing process-related aspects that lead to the efficiency improvement.

3.2.1. J_{sc} loss analysis

A J_{sc} loss analysis was carried out by measuring the external quantum efficiency (EQE) and reflectance curves of 4 median cells per batch using a Spectral Response (SR) tool with an illumination spot size of $10 \text{ mm} \times 1 \text{ mm}$. The spot was positioned between the metal fingers and therefore the EQE and reflectance curves were free from metal shading losses. The EQE and reflectance curves for each measurement were resolved into individual J_{sc} loss components, using the procedure described in (Wong et al., 2015). The J_{sc} loss components identified with this procedure are: reflectance loss due to reflectance from the anti-reflection coating (ARC), ‘blue’ loss representing the combined loss due to ARC and emitter absorption, base collection loss representing imperfect collection in the silicon wafer, near-infrared (NIR) parasitic absorption loss due to the rear surface, and front surface escape representing unabsorbed photons which are reflected from the rear surface and escape out of the front surface. The average J_{sc} loss components for all experimental groups are shown in Fig. 6.

Mod-1 cells show reduced NIR parasitic absorption relative to the baseline, which is consistent with the reduced rear contact fraction achieved by dot openings (Mod-1) compared to line openings (baseline). Comparing Mod-1 and Mod-2, no significant difference was observed in terms of J_{sc} losses. Finally, Mod-3, which implements a selective emitter structure, achieves a significantly lower blue loss than all other groups. This is due to the very lightly doped ($160 \Omega/\text{sq}$) emitter used in Mod-3, whereas all other groups use a more heavily doped ($90 \Omega/\text{sq}$) emitter. Also, the reflectance loss for Mod-3 is higher than other cell groups because the laser doping process slightly deforms the texture as shown in Fig. 4. This step marginally increases reflectance relative to the other groups. The weighted average reflectance in the 300–1000 nm range (WAR_{1000}) for Mod-3 cells was 1.3% compared to an average WAR_{1000} value of 0.9% for the other cell groups. Also note that, in an encapsulated PV module, the front surface escape component may be mostly reflected back towards the cell, therefore this loss mechanism is not very detrimental. Fig. 7 shows the IQE of the median solar cells from the baseline and the selective emitter group.

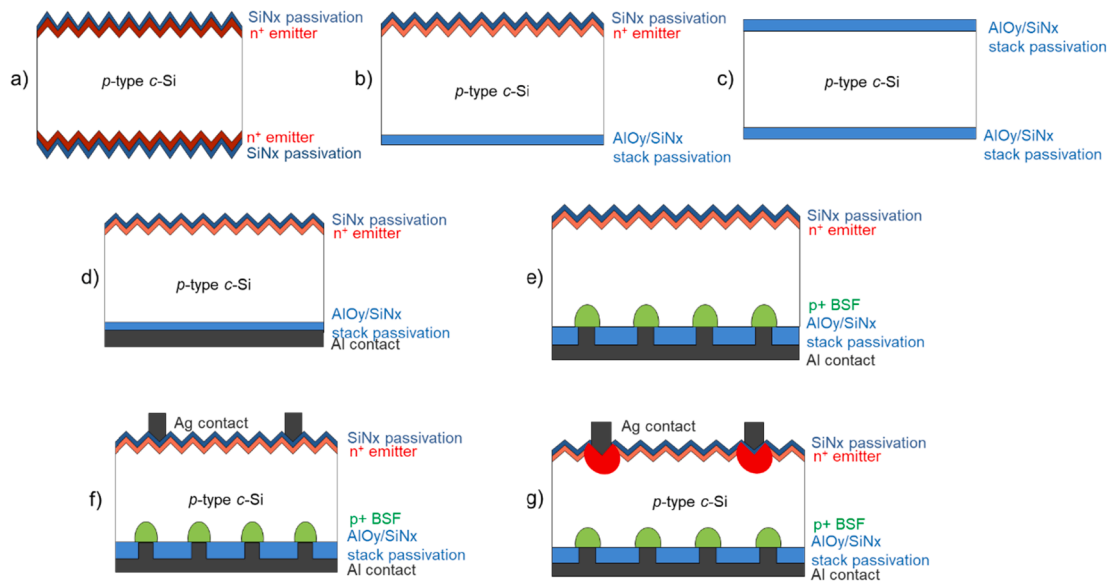


Fig. 8. Schematic of the test structures used in this work for the detailed V_{oc} loss analysis.

Table 1

Contribution of the various recombination parameters to the total recombination current density and their associated V_{oc} losses for the baseline and Mod-3 PERC solar cells.

J_0 source	Baseline PERC					Mod-3 (SE PERC)				
	J_0 [fA/cm ²]	M_f [%]	$M_f J_0$ [fA/cm ²]	iV_{oc} or V_{oc} [mV]	ΔV_{oc} [mV]	J_0 [fA/cm ²]	M_f [%]	$M_f J_0$ [fA/cm ²]	iV_{oc} or V_{oc} [mV]	ΔV_{oc} [mV]
Bulk	45					45				
Front surface passivated region	190					55				
Rear surface passivated region	15					15				
Edge and peripheral recombination	10									
Passivated cell precursor	260	–	260	666		125	–	125	685	
Front contact (Ag)	1800	5	90		–8	450	6	27		–5
Front floating busbars (Ag)			NA			400	2.5	10		–2
Rear contact (Al-full area) including influence of laser openings			100		–6			43		–6
Finished cell			450	652				205	672	

3.2.2. V_{oc} loss analysis

A detailed V_{oc} loss analysis was carried out on solar cells from the baseline and the selective emitter (Mod-3) groups. By analysing the various test structures as shown in Fig. 8, the V_{oc} loss mechanisms are quantified in terms of saturation current densities (J_0) arising from the different components of the solar cell. Selective emitter is treated as part of the front metal contact in this analysis. Hence the loss analysis samples for the Mod-3 groups are similar to the loss analysis of the baseline solar cell group.

The emitter saturation current densities (J_{0e}) of the phosphorus diffused emitters ($90 \Omega/\text{sq}$ for the baseline group and $160 \Omega/\text{sq}$ for the Mod-3 group) were determined using the high-injection method proposed by Kane & Swanson on symmetrically passivated test samples, as shown in Fig. 8a. QSSPC measurements done on passivated cell precursors (from both groups) as shown in Fig. 8b were used to extract the cells' implied V_{oc} . In order to determine the contribution of the rear side polishing ($J_{0, \text{rear}}$), textured samples were treated with the single side etch on both sides and then passivated with $\text{AlO}_y/\text{SiN}_x$ stacks, as shown in Fig. 8c. Fig. 8d is the cell precursor identical to the test structure used to extract the implied V_{oc} , except that they have screen printed aluminium (Al) metallisation on the rear side. Fig. 8e is similar to the finished solar cell except that it does not have the front metal grid. Finally, Fig. 8f and g are the finished solar cells from the baseline and the selective emitter groups. The structures in Fig. 8d–g are used to extract the V_{oc} losses associated with the screen-printed metallisation process

(contribution due to rear Al and front Ag).

The test structures and the finished solar cells from the two groups (Fig. 8d–g) were characterised by intensity-dependent PL imaging. The PL imaging system used in this work is based on a 915 nm wavelength laser as the excitation source and the illumination intensity can be varied in the range of 0.03–3.5 Suns. The loss analysis method involves high-fidelity constructions of the test pattern and the finished solar cells using an in-house finite-element method based simulator called Gridder. The Gridder modelling software finds a common set of J_0 parameters that fits both the test structures and the finished solar cells. The contribution of the various recombination parameters for the baseline and the selective emitter PERC solar cell are shown in the table below.

By analysing the test structures and the finished solar cells from the baseline and Mod-3 groups, the contribution of various recombination parameters to the total recombination density and their associated losses to V_{oc} are determined, see Table 1. The J_0 contribution of the bulk ($J_{0, \text{bulk}}$), rear surface passivated region ($J_{0, \text{rear}}$), the edge and peripheral recombination ($J_{0, \text{edge}}$) are identical for the baseline and the Mod-3 SE PERC solar cells. The massive increase in the V_{oc} of the Mod-3 SE PERC solar cells (average value of 672 mV) when compared to the baseline PERC solar cells (average value of 652 mV) arises due to improvements in the front surface passivated region, front metallisation (due to heavily diffused surface under the metal contacts and floating busbar approach), and rear metallisation (dot ablation with the laser and by using a Si containing Al paste).

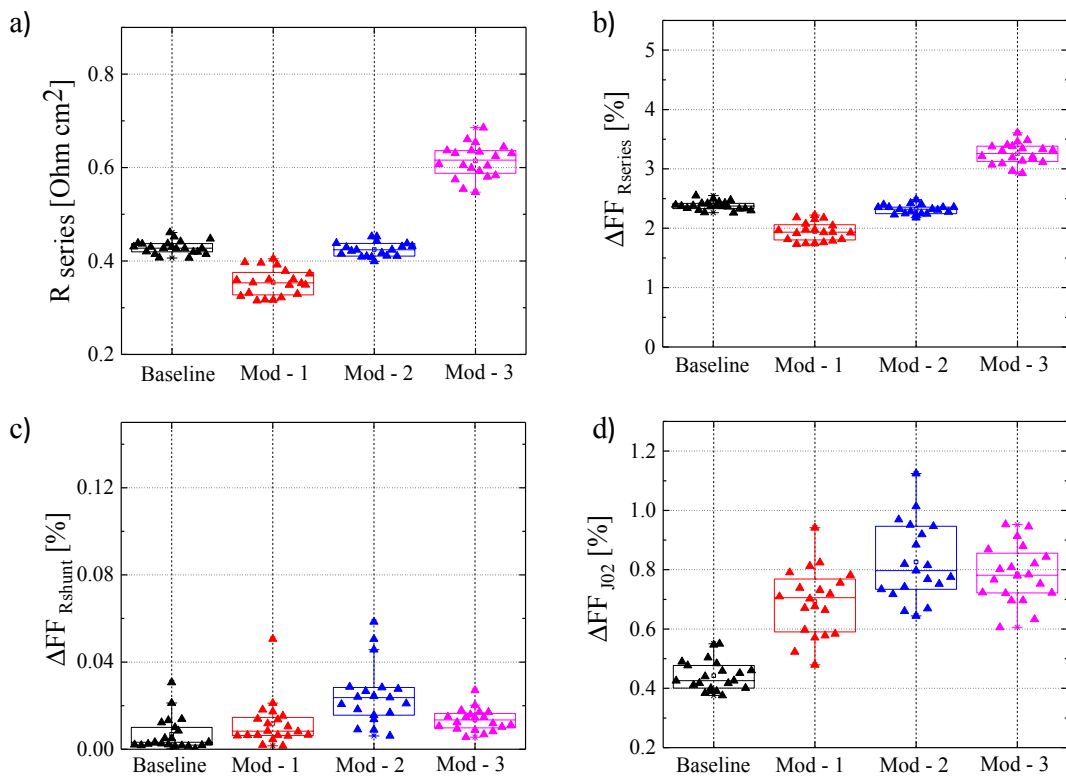


Fig. 9. FF loss analysis of the fabricated solar cells with respect to the different process modifications. The cells were all metallised with the same front grid design (105 fingers with a finger width of 35 μm). As a result of this, the SE PERC solar cells (Mod-3 group) has a higher series resistance loss when compared to the other groups.

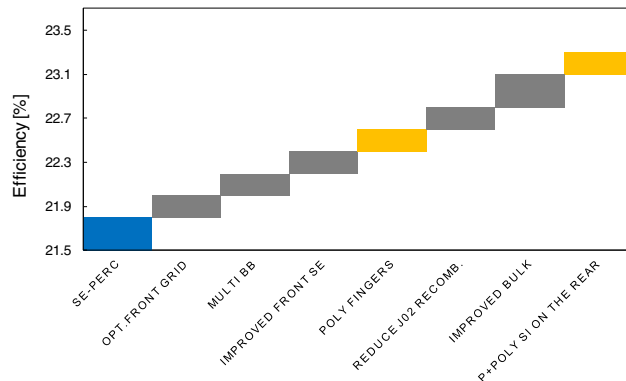


Fig. 10. A roadmap to >23.0% efficient PERC solar cells, based on the loss analysis and predicted using the Griddler software.

3.2.3. FF loss analysis

A FF loss analysis was carried out using the approach described in Ref. (Khanna et al., 2013). The cells' series resistance at the 1-Sun maximum power point (mpp) was calculated by comparing the 1-Sun I-V curve and the dark I-V curve. The shunt resistance was calculated by linearly fitting the cells' dark I-V curve in the voltage range –100 mV to 100 mV. The method described in Ref. (Wong et al., 2015) based on the two-diode model of solar cells is used to quantify the FF losses attributed to series resistance (R_s), shunt resistance (R_{sh}), and J_{02} recombination. The R_s at mpp, was around 0.6 Ωcm^2 for Mod-3 SE PERC solar cells when compared to the other groups, which were around 0.4 Ωcm^2 . This value can be reduced further for the SE PERC solar cells, by using an optimised front grid design (for a sheet resistance of 160 Ω/sq) (see Fig. 9).

3.2.4. Pathways for further efficiency improvements

Fig. 10 shows the efficiency gain analysis for the PERC solar cells, with a starting point of 21.8% for our median cell (from the Mod-3 group). Based on the loss analysis completed on these solar cells, it is evident that the FF loss due to series resistance is higher for the 21.8% SE solar cell. By re-optimising the front grid (increasing the number of front fingers to 120, and by reducing the finger width to 30 μm), the efficiency can be improved by 0.2%. The floating busbars used on these cells had a width of 700 μm . By moving towards thin busbars (100 μm in width) and a multi-BB approach (9 or 12 BB), the FF loss can be further reduced and J_{sc} can be significantly improved, leading to an efficiency of 22.2%. The next process optimization that is required will be on the front selective emitter approach. The Gaussian shaped laser beam used for doping in this work is not ideal. By using a top-hat laser beam and re-optimising the doping process, the emitter saturation current density can be reduced further. The V_{oc} loss analysis on Table 1 also shows that the $J_{02,bulk}$ is one of the largest loss mechanism in the SE PERC solar cell. By choosing wafers with improved bulk quality, the efficiency of the PERC solar cells can be improved. From our experimental study and observed cell parameter improvements, we show a pathway for the increase in PERC cell efficiency. This has many similarities to the pathways suggested by Min et al. (2017), which was based on simulation and modelling. We showed in our previous work (Padhamnath et al., 2019) that the metal contact recombination on phosphorus doped poly-Si is almost 20 times lower when compared to phosphorus doped Si surfaces. By using poly-fingers (phosphorus doped poly-Si just under the metal contacts), the metal contact recombination values can be reduced significantly (from the current values of 450 fA/cm 2 to less than 50 fA/cm 2). Once poly-Si fingers are successfully incorporated into the PERC process, the next approach to improve the efficiency will be to improve the rear side passivation and metallisation process. By integrating boron doped poly-Si at the rear surface, the loss due to Al metallisation can be reduced. These process modifications are expected to improve the

efficiency of PERC solar cells to beyond 23.0%.

4. Conclusions

This paper investigated the efficiency gains experimentally achieved in our lab with several industrially-feasible PERC improvements, leading from a baseline PERC efficiency of 20.7% to improved PERC devices with 21.9% efficiency. The key improvements presented in this paper included the transition from line to dot-shaped laser openings in the rear dielectric stack, a dual printing approach for the front fingers, and implementation of a laser-doped selective-emitter structure. A selective-emitter process using laser doping of PSG with a ns green laser source was successfully incorporated into the process flow. This resulted in a 0.3% absolute efficiency gain when compared to PERC solar cells with homogeneous phosphorus emitter. A systematic loss analysis was carried out to identify the largest power loss mechanisms in the 21.9% cells and determine the approaches for further efficiency gains. Based on experimental inputs from the loss analysis, pathways for further efficiency improvements are analysed via Griddler modelling. The modelling predicts an efficiency improvement to 22.3% via optimisation of the existing cell structure and transitioning to a multi busbar approach. Further gains in efficiency are also discussed and, by using p-type wafers with improved bulk quality and with the successful integration of poly-Si, the efficiency of these industrial PERC-like cells is expected to improve beyond 23.0%.

Declaration of Competing Interest

The authors declare that they have no known competing financial interests or personal relationships that could have appeared to influence the work reported in this paper.

Acknowledgement

SERIS is sponsored by the National University of Singapore and Singapore's National Research Foundation through the Singapore Economic Development Board. The authors would like to thank their colleagues in the Silicon Solar Cells and Modules Cluster of the Solar Energy Research Institute of Singapore (SERIS) for their assistance in sample processing and characterization.

References

- Ali, J.M.Y., Shamugam, V., Khanna, A., Wang, P., Balaji, N., Tabajonda, R.V., Perez, D.J., Aberle, A.G., Mueller, T., 2019. Analysis of nanosecond and femtosecond laser ablation of rear dielectrics of silicon wafer solar cells. *Sol. Energy Mater. Sol. Cells* 192, 117–122.
- Antoniadis, H., Jiang, F., Shan, W., Liu, Y., 2010. All screen printed mass produced silicon ink selective emitter solar cells. In: IEEE, pp. 001193–001196.
- Basu, P.K., Shetty, K.D., Vinodh, S., Sarangi, D., Palina, N., Duttagupta, S., Lin, F., Du, Z., Chen, J., Hoex, B., Boreland, M.B., Aberle, A.G., 2012. 19% efficient inline-diffused large-area screen-printed Al-LBSF silicon wafer solar cells. *Energy Procedia* 27, 444–448.
- Cuevas, A., Russell, D.A., 2000. Co-optimisation of the emitter region and the metal grid of silicon solar cells. *Prog. Photovoltaics Res. Appl.* 8 (6), 603–616.
- Dastgheib-Shirazi, A., Haverkamp, H., Raabe, B., Book, F., Hahn, G., 2008. Selective emitter for industrial solar cell production: a wet chemical approach using a single side diffusion process. In: 23rd European Photovoltaic Solar Energy Conference. EU PVSEC, pp. 1197–1199.
- Dubé, C.E., Tsefekas, B., Buzby, D., Tavares, R., Zhang, W., Gupta, A., Low, R.J., Skinner, W., Mullin, J., 2011. High efficiency selective emitter cells using patterned ion implantation. *Energy Procedia* 8, 706–711.
- Dullweber, T., Kranz, C., Peibst, R., Baumann, U., Hannebauer, H., Füll, A., Steckemetz, S., Weber, T., Kutzer, M., Müller, M., 2016. PERC+: industrial PERC solar cells with rear Al grid enabling bifaciality and reduced Al paste consumption. *Prog. Photovoltaics Res. Appl.* 24 (12), 1487–1498.
- Dullweber, T., Schmidt, J., 2016. Industrial silicon solar cells applying the passivated emitter and rear cell (PERC) concept—A review. *IEEE J. Photovoltaics* 6 (5), 1366–1381.
- Emiliano Bellini, 2020 <https://www.pv-magazine.com/2019/09/17/canadian-solar-raises-efficiency-record-for-mono-cast-cell/> (accessed 17 March 2020).
- F. Colville, 2019. <https://www.pv-tech.org/editors-blog/mono-perc-cell-production-t-o-lead-solar-industry-in-2019> (accessed 17 March 2020).
- Jianbin, F., 2019. The Roadmap to >24% PERC, PVSEC-29. Xi'an, China 2019.
- Glunz, S., Preu, R., Biro, D., Crystalline silicon solar cells-state-of-the-art and future developments.
- Hallam, B., Uruena, A., Russell, R., Aleman, M., Abbott, M., Dang, C., Wenham, S., Tous, L., Poortmans, J., 2015. Efficiency enhancement of i-PERC solar cells by implementation of a laser doped selective emitter. *Sol. Energy Mater. Sol. Cells* 134, 89–98.
- Hannebauer, H., Dullweber, T., Falcon, T., Chen, X., Brendel, R., 2013. Record low Ag paste consumption of 67.7 mg with dual print. *Energy Procedia* 43, 66–71.
- ITRPV, 2019. <https://pv-manufacturing.org/wp-content/uploads/2019/03/ITRPV-2019.pdf> (accessed 17 March 2020).
- Jäger, U., Oesterlin, P., Kimmerle, A., Preu, R., 2010. Beam shaping—the key to high throughput selective emitter laser processing with a single laser system. In: 2010 35th IEEE Photovoltaic Specialists Conference. IEEE, pp. 001401–001405.
- Kane, D., Swanson, R., 1985. Measurement of the emitter saturation current by a contactless photoconductivity decay method. In: IEEE Photovoltaic Specialists Conference, vol. 18. pp. 578–583.
- Kerr, M.J., Cuevas, A., Sinton, R.A., 2002. Generalized analysis of quasi-steady-state and transient decay open circuit voltage measurements. *J. Appl. Phys.* 91 (1), 399–404.
- Khanna, A., Mueller, T., Stangl, R.A., Hoex, B., Basu, P.K., Aberle, A.G., 2013. A fill factor loss analysis method for silicon wafer solar cells. *IEEE J. Photovoltaics* 3 (4), 1170–1177.
- Kranz, C., Wyczanowski, S., Baumann, U., Weise, K., Klein, C., Delahaye, F., Dullweber, T., Brendel, R., 2013. Wet chemical polishing for industrial type PERC solar cells. *Energy Procedia* 38, 243–249.
- Kray, D., Aleman, M., Fell, A., Hopman, S., Mayer, K., Mesec, M., Müller, R., Willeke, G., Glunz, S., Bitnar, B., 2008. Laser-doped silicon solar cells by laser chemical processing (LCP) exceeding 20% efficiency. In: 2008 33rd IEEE Photovoltaic Specialists Conference. IEEE, pp. 1–3.
- König, M., Deckelmann, M., Henning, A., Hoenig, R., Clement, F., Hřeiteis, M., 2012. Dual screen printing featuring novel framed busbar screen layout and non-contacting Ag busbar paste. *Energy Procedia* 27, 510–515.
- Lauermann, T., Dastgheib-Shirazi, A., Book, F., Raabe, B., Hahn, G., Haverkamp, H., Habermann, D., Demberger, C., Schmid, C., 2009. InSECT: an inline selective emitter concept with high efficiencies at competitive process costs improved with inkjet masking technology. In: 24th European Photovoltaic Solar Energy Conference. pp. 1767–1770.
- Lorenz, A., Linse, M., Frintrup, H., Jeitler, M., Mette, A., Lehner, M., Greutmann, R., Brocker, H., König, M., Erath, D., 2018. Screen printed thick film metallization of silicon solar cells-recent developments and future perspectives. In: 35th European Photovoltaic Solar Energy Conference and Exhibition. pp. 819–824.
- Lv, Y., Zhuang, Y., Wang, W., Wei, W., Sheng, J., Zhang, S., Shen, W., 2020. Towards high-efficiency industrial p-type mono-like Si PERC solar cells. *Sol. Energy Mater. Sol. Cells* 204, 110202.
- Mark Hutchins, 2018. <https://www.pv-magazine.com/2018/05/09/jinkosolar-achieves-23-95-efficiency-for-p-type-mono-cell/> (accessed 17 March 2020).
- Mark Osborne, 2019. <https://www.pv-tech.org/news/longi-solar-has-bifacial-mono-perc-solar-cell-world-record-verified-at-24.0> (accessed 17 March 2020).
- Mark Osborne, 2020. <https://www.pv-tech.org/news/trina-solar-hits-23.39-efficiency-for-industrial-perc-cell> (accessed 17 March 2020).
- Min, B., Müller, M., Wagner, H., Fischer, G., Brendel, R., Altermatt, P.P., Neuhaus, H., 2017. A roadmap toward 24% efficient PERC solar cells in industrial mass production. *IEEE J. Photovoltaics* 7 (6), 1541–1550.
- Müller, M., Fischer, G., Bitnar, B., Steckemetz, S., Schiepe, R., Mühlbauer, M., Köhler, R., Richter, P., Kusterer, C., Oehlike, A., 2017. Loss analysis of 22% efficient industrial PERC solar cells. *Energy Procedia* 124, 131–137.
- Padhamnath, P., Wong, J., Nagarajan, B., Buatis, J.K., Ortega, L.M., Nandakumar, N., Khanna, A., Shamugam, V., Duttagupta, S., 2019. Metal contact recombination in monoPoly™ solar cells with screen-printed & fire-through contacts. *Sol. Energy Mater. Sol. Cells* 192, 109–116.
- Preu, R., Glunz, S., Schäfer, S., Lüdemann, R., Wetling, W., Pfleging, W., 2000. Laser ablation—a new low-cost approach for passivated rear contact formation in crystalline silicon solar cell technology. In: Proceedings of the 16th European Photovoltaic Solar Energy Conference, pp. 1181–1184.
- Röder, T., Eisele, S., Grabitz, P., Wagner, C., Kulushich, G., Köhler, J., Werner, J., 2010. Add-on-laser tailored selective emitter solar cells. *Prog. Photovoltaics Res. Appl.* 18 (7), 505–510.
- Röder, T., Grabitz, P., Eisele, S., Wagner, C., Köhler, J., Werner, J., 2009. 0.4% absolute efficiency gain of industrial solar cells by laser doped selective emitter. In: 2009 34th IEEE Photovoltaic Specialists Conference (PVSC). IEEE, pp. 000871–000873.
- Safiez, A., Wolter, K., Nagel, M., Windgassen, H., Kurz, H., 2013. Evaluation and investigation of laser doping by a double-gaussian shaped beam profile. In: 2013 IEEE 39th Photovoltaic Specialists Conference (PVSC). IEEE, pp. 2263–2267.
- Shamugam, V., Cunnusamy, J., Khanna, A., Basu, P.K., Zhang, Y., Chen, C., Stassen, A., F., Boreland, M.B., Mueller, T., Hoex, B., Aberle, A.G., 2014. Electrical and microstructural analysis of contact formation on lightly doped phosphorus emitters using thick-film Ag screen printing pastes. *IEEE J. Photovoltaics* 4 (1), 168–174.
- Shamugam, V., Khanna, A., Basu, P.K., Aberle, A.G., Mueller, T., Wong, J., 2016. Impact of the phosphorus emitter doping profile on metal contact recombination of silicon wafer solar cells. *Sol. Energy Mater. Sol. Cells* 147, 171–176.
- Shamugam, V., Khanna, A., Perez, D.J., Tabajonda, R.V., Yacob Ali, J.M., Ortega, A.L. M., Garcia, I.J., Lim, B., Mueller, T., 2018. 21% efficient screen-printed n-type silicon wafer solar cells with implanted phosphorus front surface field. *Sol. Energy Mater. Sol. Cells* 186, 124–130.
- Shamugam, V., Wong, J., Peters, I.M., Cunnusamy, J., Zahn, M., Zhou, A., Yang, R., Chen, X., Aberle, A.G., Mueller, T., 2015. Analysis of fine-line screen and stencil-

- printed metal contacts for silicon wafer solar cells. *IEEE J. Photovoltaics* 5 (2), 525–533.
- Shetty, K.D., Boreland, M.B., Shanmugam, V., Cunnusamy, J., Wu, C.-K., Iggo, S., Antoniadis, H., 2013. Lightly doped emitters for high efficiency silicon wafer solar cells. *Energy Procedia* 33, 70–75.
- Stenzel F., Lee B.G., Cieslak J., Schwabedissen A., Wissen D., Geißler S., Rudolph T., Faulwetter-Quandt B., Höning R., Wasmer S., Bakowskie R., Buß D., Fertig F., Schaper M., Mette A., Müller J.W., 2019, Exceeding 23% and mass production of p-Cz Quantum bifacial solar cells. In: Proc. 36th Europ. Photovolt. Solar Energy Conf., 2019, pp. 96–99.
- Strinitz, F., El Jaouhari, A., Schoerg, F., Fuerst, M., Plettig, M., Kuehnlein, H., 2017. Advanced alkaline texturing and cleaning for PERC and SHJ solar cells. *Energy Procedia* 130, 23–30.
- Tsuji, K., Suzuki, S., Morishita, N., Kuroki, T., Nakahara, M., Dhamrin, M., Peng, W., Buck, T., Usami, N., 2019. Fine line Al printing on narrow point contact opening for front side metallization. *AIP Con Proc* 2147 (2019), 040019.
- Wagner, H., Dastgheib-Shirazi, A., Min, B., Morishige, A.E., Steyer, M., Hahn, G., del Cañizo, C., Buonassisi, T., Altermatt, P.P., 2016. Optimizing phosphorus diffusion for photovoltaic applications: peak doping, inactive phosphorus, gettering, and contact formation. *J. Appl. Phys.* 119 (18), 185704.
- Werner, S., Lohmüller, E., Saint-Cast, P., Greulich, J., Weber, J., Schmidt, S., Moldovan, A., Brand, A., Dannenber, T., Mack, S., 2017. Key aspects for fabrication of p-type Cz-Si PERC solar cells exceeding 22% conversion efficiency. In: Proceedings of the the 33rd European PV Solar Energy Conference and Exhibition, Amsterdam, The Netherlands. pp. 25–29.
- Wong, J., Duttagupta, S., Stangl, R., Hoex, B., Aberle, A.G., 2015. A systematic loss analysis method for rear-passivated silicon solar cells. *IEEE J. Photovoltaics* 5 (2), 619–626.
- Wu, W., Zhang, Z., Zheng, F., Lin, W., Liang, Z., Shen, H., 2018. Efficiency enhancement of bifacial PERC solar cells with laser doped selective emitter and double screen printed Al grid. *Prog. Photovoltaics Res. Appl.* 26 (9), 752–760.
- Yichun, W., Tian, X., 2018. Supply of low-cost and high-efficiency multi-GW mono wafers. *Photovoltaics Int.* 38–42.